Journal of Machine Engineering, 2023, Vol. 23
ISSN 1895-7595 (Print) ISSN 2391-8071 (Online)

Received: *04 April 2023* / Accepted: *13 May 2023* / Published online: *15 May 2023*

wire-arc directed energy deposition,
weld tracks, ER308L stainless steel,
multi-objective optimization

Van Canh NGUYEN[1], Van Thao LE[2*],
Ngoc-Linh PHAM[1], Anh-Thang NGUYEN[3]

MULTI-OBJECTIVE OPTIMIZATION FOR WELD TRACK GEOMETRY IN WIRE-ARC DIRECTED ENERGY DEPOSITION OF ER308L STAINLESS STEEL

In this research, the weld track geometry in wire-arc DED (directed energy deposition) of ER308L stainless steel was predicted and optimized. The studied geometrical attributes of weld tracks include weld track width (*WTW*), weld track height (*WTH*), and contact angle (α). The experiment was designed based on Taguchi method with three variables (current *I*, voltage *U*, and weld velocity *v*) and four levels for each variable. The ANOVA was adopted to evaluate the accuracy of the models and impact levels of variables on the responses. The TOPSIS method was utilized to predict the optimal variables. The results indicated that the predicted models were built with high accuracy levels (R^2 = 98.92%, 98.77%, and 98.91% for *WTW*, *WTH*, and α, respectively). Among the studied variables, *U* features the highest effects on *WTW* and α with 78.56% and 69.90% of contribution, respectively, while *v* is the variable that has the most impact on *WTH* with 39.82% of contribution. The optimal variables predicted by TOPSIS were *U* = 23 V, *I* = 140 A, and *v* = 300 mm/min, which allows building components with stable and regular geometry.

1. INTRODUCTION

Wire-arc directed-energy deposition (DED) is being adopted as a promising additively manufacturing technique for fabricating large-size metallic components in different industrial areas, such as aviation, shipbuilding, and construction [1]. The wire-arc DED process uses an arc source to fuse a metallic wire, and the molten metal is deposited into the part layer-by-layer. This technology introduces several unique characteristics such as elevated deposition rates and high utilization efficiency of materials [2]. The arc sources used in the wire-arc DED process could be gas tungsten arc welding (GTAW), gas metal arc welding (GMAW), and plasma arc welding (PAW) [3]. However, the GMAW-DED process is the most preferrable for manufacturing large-scale metal parts thanks to its capacity of depositing materials at high rates, about 8 kg/h [4].

In wire-arc DED processes, the geometry of weld tracks significantly affects the print-ability and the final forming quality of components. The geometrical attributes of single weld

[1] Faculty of Mechanical Engineering, Hanoi University of Industry, Vietnam
[2] Advanced Technology Center (ATC), Le Quy Don Technical University, Vietnam
[3] Vietnam-Japan Center, Hanoi University of Industry, Vietnam
[*] E-mail: vtle@lqdtu.edu.vn
http://doi.org/10.36897/jme/166134

tracks, such as weld track width (*WTW*), weld track height (*WTH*), and contact angle (α) are elementary variables for generating printing paths in the wire-arc DED process. Hence, a number of studies has focused on building the predictive models of the geometrical attributes of single weld tracks and investigated the effects of process variables on the weld track attributes. Suryakumar et al. [5] built the models of *WTW* and *WTH* for single weld tracks of ER70S6 filler material. Wang et al. [6] utilized an ANN model to forecast the shape of weld tracks based on wire-feed velocity, traveling speed, and interlayer temperature in the GMAW-DED process. Similarly, Geng et al. [7] used the response surface methodology (RSM) to anticipate the weld track shape in GTAW-DED of 5A06 aluminum alloy. Meanwhile, Youheng et al. [8] examined how the wire-feed velocity and traveling speed affected *WTW* and *WTH*, and discovered optimal process variables for creating weld track with stable shape and less spatter in wire-arc DED of bainitic steels. Sarathchandra et al. [9] researched the impact of process variables on geometry attributes of SS304 weld tracks fabricated by wire-arc DED. They utilized the RSM and DA methods to identify optimal processing variables. Kumar and Maji [10] built geometrical models of weld tracks in wire-arc DED of SS304L and predicted optimal process variables to obtain expected weld track geometry utilizing the RSM and desirability function (DF) methods. Venkatarao [11] adopted the teaching-learning-based optimization (TLBO) algorithm to identify the optimal weld track in wire-arc DED of low-carbon steels. They demonstrated that TLBO was more powerful to predict optimal process variables than Taguchi and RMS methods.

From the above survey, it is apparent that the impact of process variables on the geometry features of weld tracks in wire-arc DED of ER308L steel was rarely investigated. ER308L stainless steel is extensively utilized in various sectors such as gas, oil, mining, and automotive industries due to its low percentage of carbon content. Typically, the wire-arc DED of ER308L components were performed using the processing variables suggested by welding wire producers for traditional welding techniques, while the weld track geometry plays an important role for the design of printing paths. Therefore, this study aims to forecast the geometry attributes of weld tracks and determine the optimal process variables for the wire-arc DED of ER308L steel. The predictive models for the weld track attributes can be used for the printing path generation as well as for the prediction of variables corresponding to target responses. The experiments were designed using the L16-orthogonal-array Taguchi method, taking into account three process variables, including current *I*, voltage *U*, and travel speed *v*. The geometrical responses were the weld track width (*WTW*), weld track height (*WTH*), and contact angle (α). The optimal process variables were predicted by the techniques for order-preferences by similarity-to-Ideal solution (TOPSIS). The analysis of variance (ANOVA) was also adopted to identify the significance and effects of each input variable on the responses.

2. MATERIALS AND METHODS

2.1. MATERIALS AND EXPERIMENT DESIGN

In this article, 1.2-mm-diameter weld wire of ER308L steel and the substrates made of A36 steel with dimensions of 150 mm × 150 mm × 10 mm were utilized in the wire-arc

DED process. The chemical elements of the ER308L wire are composed of Ni (9 ~ 11 %), Cr (19.5 ~ 21%), Mn (1 ~2.5%), Mo (≤ 0.5%), Si (0.3 ~ 0.65%), Cu (≤ 0.75%), P/C/S (≤ 0.03%), and balanced % Fe. The mechanical properties of the ER308L steel are ~ 390 MPa in yield strength, ~ 580 MPa in ultimate tensile strength, and ~ 40% in elongation. The wire and arc DED system is composed of an industrial Panasonic robot, a welding power source (YD350 GR3), a system of wire feeding, and a shielding gas feeding (Fig. 1a). The shielding gas used to protect the melting pool in the wire and arc DED process was pure argon with a flow rate of 18 L/min.

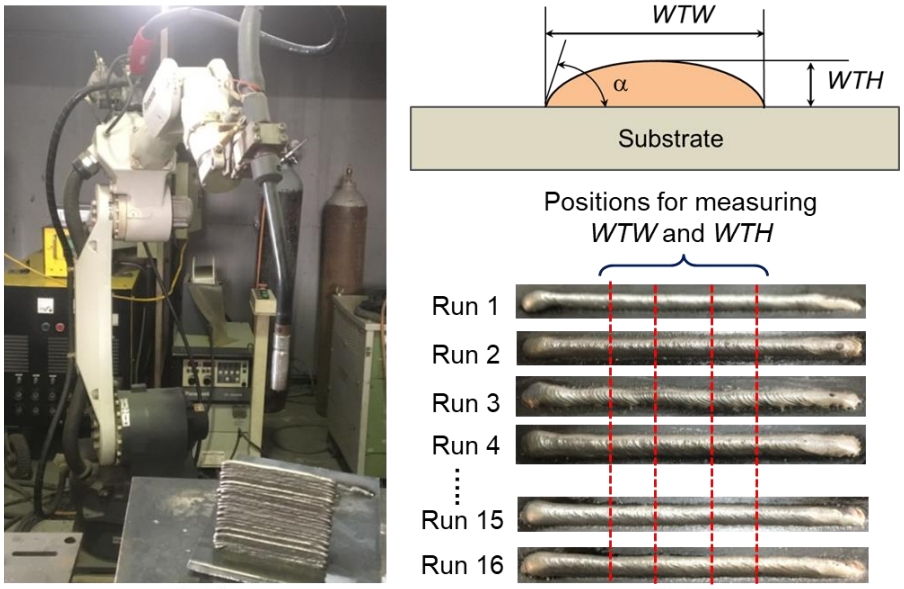

(a) (b)

Fig. 1. (a) GMAW-DED system and (b) single weld track and its geometry attributes

In the GMAW-DED process, *U*, *I*, and *v* are the main operating parameters, and they significantly influence the weld bead geometry, whereas other parameters such as the flow rate of shielding gas and distance from the contact tip to the substrate have less impact. Hence, in this study, the process parameters *U*, *I*, and *v* were the input variables, while the responses of single weld tracks were the weld track width (*WTW*), weld track height (*WTH*), and contact angle (α). Each input variable has four levels, and their values were shown in Table 1. The L16-orthogonal Taguchi method was adopted to design the experiment. Therefore, the experiment includes 16 trials of weld tracks. The weld track length is about 80 mm. The distance between the adjacent weld track was 20 mm. After a run of a weld track, the substrate was rapidly cooled down to room temperature using compressed air. The *WTW* and *WTH* of single weld tracks were measured at four positions in a stable zone (Fig. 1b) using a digital Mitutoyo calliper with ± 0.02 mm in precision and 0.01 mm in resolution. The contact angle (α) was computed by Eq. (1) [6], and the heat input was calculated by Eq. (2), where η is the arc efficiency ratio, η = 0.8 [3]. The results of measurement and calculation were presented in Table 2.

$$\alpha = \frac{180}{\pi} \times 2 \times \arctan\left(\frac{2 \times WTH}{WTW}\right) \tag{1}$$

$$E_l = 60 \times \eta \times \frac{U \times I}{v} \tag{2}$$

Table 1. Studied wire and arc DED variables and their levels

Variables	Level-1	Level-2	Level-3	Level-4
U (V)	17	19	21	23
I (A)	110	120	130	140
v (mm/min)	300	350	400	450

Table 2. Experiment runs and the measured responses

No	U (V)	I (A)	v (mm/min)	WTW (mm)	WTH (mm)	α (deg.)	E_l (J/mm)
1	17	110	300	4.06	3.78	124	374
2	19	110	350	4.74	3.16	106	358
3	21	110	400	4.94	2.88	99	347
4	23	110	450	5.16	2.54	89	337
5	17	120	350	4.23	3.91	123	350
6	19	120	300	4.98	3.65	111	456
7	21	120	450	4.83	2.90	100	336
8	23	120	400	5.12	2.88	97	414
9	17	130	400	4.10	3.83	124	332
10	19	130	450	4.25	3.12	111	329
11	21	130	300	5.36	3.96	112	546
12	23	130	350	5.18	3.34	104	513
13	17	140	450	3.85	3.74	126	317
14	19	140	400	4.54	3.73	117	399
15	21	140	350	5.26	3.81	111	504
16	23	140	300	5.76	4.15	110	644

2.2. OPTIMIZATION PROBLEM

As mentioned above, the TOPSIS was used to identify the optimal set of process variables in the wire and arc DED process of ER308L stainless steel. The problem of multi-attribute optimization was described as: "Find {U, I, v} that maximize {WTW and WTH} while minimize (α), subject to $17 \leq U \leq 22$ V, $110 \leq I \leq 140$ A, and $300 \leq v \leq 450$ mm/min."

In TOPSIS method [12], the attributes (i.e., WTW, WTH, and α) were firstly placed in the deciding matrix $\mathbf{DM} = [A_{ij}]_{mxn}$, where A_{ij} is the j^{th} objective in the i^{th} experimental run, n is the objectives number, and m is the experimental runs number.

The deciding matrix **DM** was then normalized using Eq. (3):

$$a_{ij} = \frac{A_{ij}}{\sqrt{\sum_{i=1}^{m} A_{ij}^2}} \tag{3}$$

Subsequently, the weights ω_j, where $\omega_j \in (0, 1)$ and $\sum_{j=1}^{n} \omega_j = 1$ were used to calculate the weighted-normalized-deciding matrix, as Eq. (4):

$$v_{ij} = \omega_j \cdot a_{ij} \tag{4}$$

After that the unideal solutions (S_-) and ideal solutions (S_+) were identified by Eq. (5) and Eq. (6):

$$S^- = \{(\min_i v_{ij} \mid j \in J), (\max_i v_{ij} \mid j \in J), i = 1, 2, ..., m\} = \{S_1^-, S_2^-, ..., S_n^-\} \tag{5}$$

$$S^+ = \{(\max_i v_{ij} \mid j \in J), (\min_i v_{ij} \mid j \in J), i = 1, 2, ..., m\} = \{S_1^+, S_2^+, ..., S_n^+\} \tag{6}$$

The viable solution distances from S^- or S^+ were calculated by Eq. (7) and Eq. (8):

$$D_i^- = \sqrt{\sum_{j=1}^{n} (v_{ij} - S_j^-)^2} \tag{7}$$

$$D_i^+ = \sqrt{\sum_{j=1}^{n} (v_{ij} - S_j^+)^2} \tag{8}$$

Lastly, the closest degree of ideal solution CS_i is calculated by Eq. (9):

$$CS_i = \frac{D_i^-}{D_i^- + D_i^+} \tag{9}$$

The optimal solution is selected based on the highest CS_i value.

3. RESULTS AND DISCUSSION

3.1. PROCESS VARIABLE EFFECTS ON THE WELD TRACK ATTRIBUTES

The effects of process variables on the weld track width (*WTW*) were shown in Fig. 2. It is revealed that when *I* increased from 110 A to 140 A, *WTW* show a slight increasing tendency. On the other hand, *WTW* significantly increases with an increment in *U* from 17 V to 23 V. The effect of *v* on *WTW* is opposite to those of *U* and *I*. *WTW* decreases when *v* increases from 300 mm/min to 450 mm/min. In fact, when *I* increased, the wire feed speed and material deposition volume also increased, causing the melting pool size and *WTW* to increase [9]. Additionally, increasing *U* leads to a longer and wider arc, resulting in a larger *WTW*. Conversely, if *v* increased, the amount of material deposition per unit length decreases, causing *WTW* to narrow [9]. The effect tendency of the variables *U*, *I*, and *v* on WTW is in line with previous works [9, 13].

The results of analysis of variance (ANOVA) for *WTW* was shown in Table 3. The predictive model of *WTW* is described by Eq. (10). The determining coefficients' model are R^2 = 98.92%, R^2_adj = 97.29%, and R^2_pred = 88.06%, indicating the *WTW* model has elevated precision. The ANOVA results also indicate that the significant terms of the model are *U*, *v*, U^2, and $U{\cdot}v$, which feature a P-value inferior to 0.05, and other terms of the model are insignificant, which can be excluded from the model when predicting *WTW*. According to the ANOVA results, *U* reveal the most important impact level on *WTW* with a percentage contribution of 78.56%, followed by *v* with a contribution of 13.30%. On the other hand, the level impact of *I* on *WTW* is very low, with a percentage contribution of 0.43%. These results agree with the impact tendency of *I* and *U* on *WTW* displaying in Fig. 2.

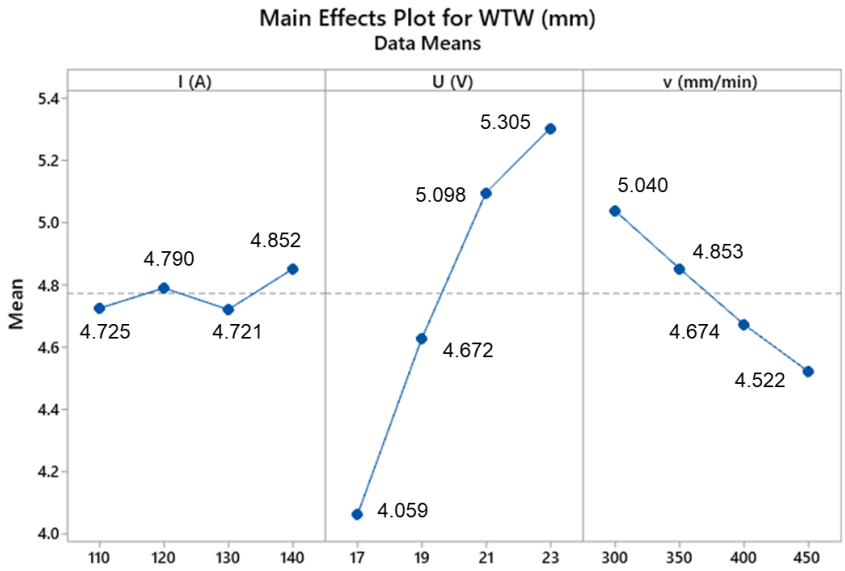

Fig. 2. Main effect of process variables on *WTW*

$$WTW\ (\text{mm}) = -21.94 + 0.1052{\cdot}I + 1.422{\cdot}U + 0.0276{\cdot}v + 0.000163{\cdot}I^2 - 0.02252{\cdot}U^2 + 0.000003{\cdot}v^2 - 0.00249{\cdot}I{\cdot}U - 0.000252{\cdot}I{\cdot}v - 0.000151{\cdot}U{\cdot}v \quad (10)$$

Table 3. ANOVA results related to *WTW*

Source	DF	Seq SS	Contribution	Adj SS	Adj MS	F-Value	P-Value	Remark
Regression	9	4.46151	98.92%	4.46151	0.495724	60.80	0.000	Significant
I (A)	1	0.01929	0.43%	0.01943	0.019432	2.38	0.174	No Significant
U (V)	1	3.54358	78.56%	0.16406	0.164056	20.12	0.004	Significant
v (mm/min)	1	0.59988	13.30%	0.04393	0.043933	5.39	0.050	Significant
I^2	1	0.00426	0.09%	0.00426	0.004262	0.52	0.497	No significant
U^2	1	0.12978	2.88%	0.12978	0.129778	15.92	0.007	Significant
v^2	1	0.00117	0.03%	0.00117	0.001175	0.14	0.717	No significant
$I{\cdot}U$	1	0.02177	0.48%	0.02177	0.021774	2.67	0.153	No significant
$I{\cdot}v$	1	0.13976	3.10%	0.13976	0.139764	17.14	0.006	Significant
$U{\cdot}v$	1	0.00200	0.04%	0.00200	0.002001	0.25	0.638	No significant
Error	6	0.04892	1.08%	0.04892	0.008153			
Total	15	4.51043	100.00%					

Figure 3 presents the direct influence of process variables on the weld track height (*WTH*). It can be found that *WTH* increased when *I* increased from 110 A to 140 A. On the other hand, *WTH* decreased when both *U* and *v* increased. This effect trend of *U*, *I*, and *v* on WTW is also good in agreement with previous studies [9, 13, 14]. In fact, when the current *I* raised, the wire feed speed also went up. This leads to an increase in the amount of material deposited, resulting in a higher *WTH* [13]. Additionally, an increase in *I* causes weld beads to become more convex, further increasing *WTH*. Conversely, when *v* increased, the amount of deposited material per unit length decreased, resulting in a reduction in the *WTH* [9]. When the voltage is increased, the arc's spreading area becomes wider, resulting in flatter weld beads [14]. Therefore, an increase in voltage is associated with a reduction in *WTH*.

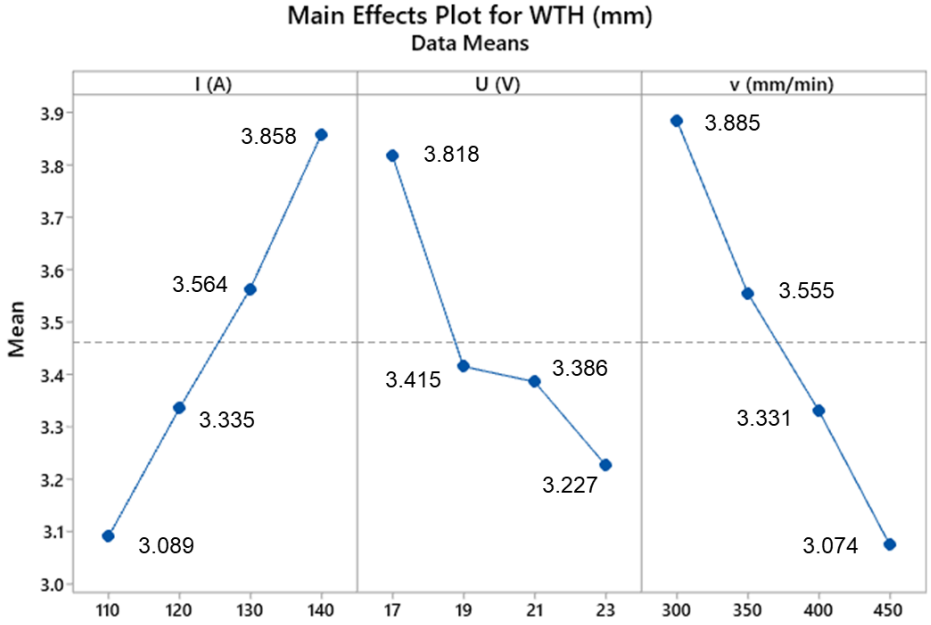

Fig. 3. Main impact of processing variables on *WTH*

The results of ANOVA related to *WTH* was presented in Table 4. It is indicated that *v* has the most important contribution on *WTH* with an effect contribution of 39.82%, followed by *I* and *U* with an effect contribution of 36.21% and 18.29%, respectively. The ANOVA analysis results agree with those displayed in Fig. 3. The prediction model of *WTH* was described by Eq. (11). The determination coefficients of the model, R^2 = 98.77%, R^2_pred = 87.52%, R^2_adj = 96.92%, express that the model features a high accurate level, and it can be utilized for predicting the weld track height in the whole space of experimental design. Moreover, in the predictive model, the terms *I*, *U*, *v*, U^2, $I \cdot v$ are significant because they showed the P-value inferior to 0.05. Meanwhile, other terms with the P-value higher than 0.05 are insignificant and they can be excluded from the predictive model of *WTH*.

$$WTH\ (\text{mm}) = 4.06 + 0.0705 \cdot I - 0.722 \cdot U + 0.0155 \cdot v + 0.000123 \cdot I^2 + 0.01522 \cdot U^2 + 0.000007 \cdot v^2 - 0.00002 \cdot I \cdot U - 0.000202 \cdot I \cdot v - 0.000054 \cdot U \cdot v \quad (11)$$

Table 4. ANOVA results related to *WTH*

Source	DF	Seq SS	Contribution	Adj SS	Adj MS	F-Value	P-Value	Remark
Regression	9	3.50215	98.77%	3.50215	0.389128	53.37	0.000	Significant
I (A)	1	1.28402	36.21%	0.00873	0.008728	1.20	0.031	Significant
U (V)	1	0.64856	18.29%	0.04231	0.042307	5.80	0.050	Significant
v (mm/min)	1	1.41195	39.82%	0.01385	0.013847	1.90	0.022	Significant
I^2	1	0.00240	0.07%	0.00240	0.002402	0.33	0.587	No significant
U^2	1	0.05932	1.67%	0.05932	0.059325	8.14	0.029	Significant
v^2	1	0.00550	0.16%	0.00550	0.005502	0.75	0.418	No significant
I·*U*	1	0.00000	0.00%	0.00000	0.000001	0.00	0.990	No significant
I·*v*	1	0.09015	2.54%	0.09015	0.090146	12.36	0.013	Significant
U·*v*	1	0.00025	0.01%	0.00025	0.000253	0.03	0.858	No significant
Error	6	0.04375	1.23%	0.04375	0.007291			
Total	15	3.54590	100.00%					

Figure 4 displays the main impact of the variables on the contact angle (α). It can be found that α reduced when *U* and *v* augmented. This observation is similar to that observed in the literature [15]. Indeed, as *U* increases, *WTW* increased while *WTH* decreased. As a result, α decreased. When *v* increased, the heat input and the quantity of deposited metal in a unit of length reduced. Hence, α decreased [15]. On the other hand, α increased as the current *I* increased from 110 A to 140 A. This is due to *WTH* increases more sharply than the increase in *WTW* when *I* increased (Fig. 2 and Fig. 3). Thereby, α augmented.

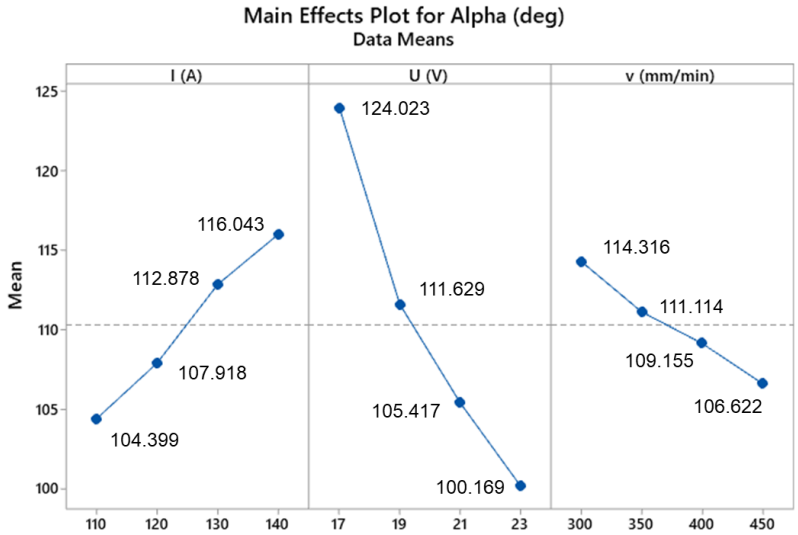

Fig. 4. Main effect of process variables on α (alpha)

Table 5 presents the results of ANOVA for the contact angle α. It is indicated that the variable *U* has the most impacting level on the contact angle α with a contribution of 69.90%, followed by I and v with the impact contribution of 18.39% and 7.26%, respectively. The predictive model of α, Eq. (12), also shows an acceptable accuracy with high values of determination coefficients, with high determination coefficients, R^2 = 98.91%, R^2_adj =

97.28%, R^2_pred = 88.98%. Thus, this model can be used to predict the contact angle within the design space. Moreover, the terms U, I, v, U^2 with the P-value inferior to 0.5 are significant, while other terms with the P-value higher than 0.05 are insignificant. The insignificant model term can be excluded when predicting the contact angle (α).

$$\alpha\,(\text{deg.}) = 429 - 0.37\cdot I - 26.03\cdot U - 0.092\cdot v - 0.00089\cdot I^2 + 0.447\cdot U^2 + 0.000064\cdot v^2 + 0.0410\cdot I\cdot U + 0.00039\cdot I\cdot v - 0.00202\cdot U\cdot v \tag{12}$$

Table 5. ANOVA results related to the contact angle (α)

Source	DF	Seq SS	Contribution	Adj SS	Adj MS	F-Value	P-Value	Remark
Regression	9	1712.05	98.91%	1712.05	190.227	60.55	0.000	Significant
I (A)	1	318.29	18.39%	0.23	0.234	0.07	0.040	Significant
U (V)	1	1209.82	69.90%	55.00	55.005	17.51	0.006	Significant
v (mm/min)	1	125.72	7.26%	0.49	0.490	0.16	0.041	Significant
I^2	1	0.13	0.01%	0.13	0.125	0.04	0.848	No significant
U^2	1	51.08	2.95%	51.08	51.076	16.26	0.007	Significant
v^2	1	0.41	0.02%	0.41	0.409	0.13	0.730	No significant
$I\cdot U$	1	5.92	0.34%	5.92	5.916	1.88	0.219	No significant
$I\cdot v$	1	0.34	0.02%	0.34	0.341	0.11	0.753	No significant
$U\cdot v$	1	0.36	0.02%	0.36	0.359	0.11	0.747	No significant
Error	6	18.85	1.09%	18.85	3.141			
Total	15	1730.89	100.00%					

3.2. OPTIMIZATION RESULTS

The calculation results by the TOPSIS method were shown in Table 6. In this study, the weight assigned to each attribute (*WTW*, *WTH*, and α) was identical (i.e., $\omega_{(WTW)} = \omega_{(WTH} = \omega_{(\alpha)} = 1/3$).

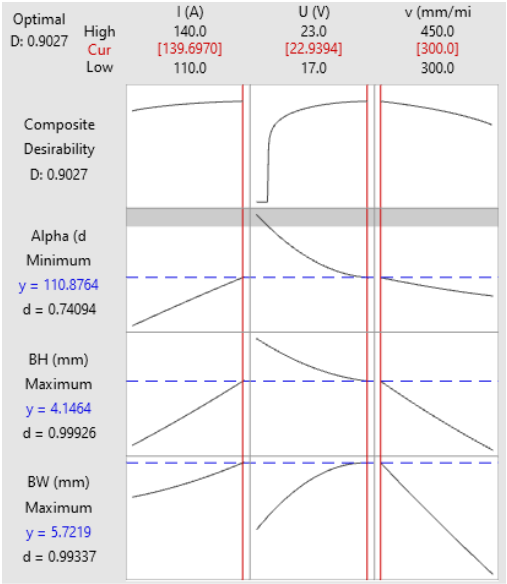

Fig. 5. Optimal solution obtained by the DF method

The ideal solutions (S_+) and unideal solution (S_-) for each attribute are {$S_+^{(WTW)}$ = 0.100, $S_-^{(WTW)}$ = 0.067}, {$S_+^{(WTH)}$ = 0.099, $S_-^{(WTH)}$ = 0.061} and {$S_+^{(\alpha)}$ = 0.067, $S_-^{(\alpha)}$ = 0.094}. The feasible solutions' distances from S_+ or S_- (i.e., D_-^i and D_+^i), and the closest degree of ideal solution CS_i were calculated by Eq. (6), Eq. (7), and Eq. (8), respectively. From the values of CS_i (Table 6), it is revealed that the Run 16 corresponds to the highest value of CS, and it is assigned at the first rank. Thus, the process variables of the run 16, {U = 23 V, v = 300 mm/min, and I = 140 A} are the optimal variables, and the weld track attributes in this case were WTW = 5.76 mm, WTH = 4.15 mm, and α = 110 deg. Figure 5 displays the optimal results obtained by the desirability function (DF) method and Minitab software. It is also revealed the nearly identical optimal solution as TOPSIS method. As a result, it can be concluded that the optimal process variables for the expected attributes of single weld track were U = 23 V, v = 300 mm/min, and I = 140 A.

Table 6. Results obtained from TOPSIS method

Run	Normalized-deciding Matrix			Weighted-Normalized-Deciding Matrix			D_i^+	D_i^-	CS_i	Rank
	WTW (mm)	WTH (mm)	α (deg)	WTW (mm)	WTH (mm)	α (deg)				
1	0.211	0.271	0.279	0.070	0.090	0.093	0.040	0.030	0.426	14
2	0.247	0.226	0.240	0.082	0.075	0.080	0.032	0.026	0.446	11
3	0.257	0.206	0.223	0.086	0.069	0.074	0.034	0.029	0.457	10
4	0.269	0.182	0.201	0.090	0.061	0.067	0.040	0.036	0.473	9
5	0.220	0.280	0.278	0.073	0.093	0.093	0.037	0.034	0.473	8
6	0.259	0.261	0.251	0.086	0.087	0.084	0.025	0.035	0.584	4
7	0.251	0.207	0.226	0.084	0.069	0.075	0.035	0.027	0.435	13
8	0.267	0.206	0.218	0.089	0.069	0.073	0.033	0.032	0.494	7
9	0.213	0.274	0.279	0.071	0.091	0.093	0.040	0.031	0.440	12
10	0.221	0.223	0.252	0.074	0.074	0.084	0.040	0.019	0.322	16
11	0.279	0.284	0.252	0.093	0.095	0.084	0.019	0.044	0.699	2
12	0.270	0.239	0.236	0.090	0.080	0.079	0.025	0.034	0.580	5
13	0.200	0.268	0.283	0.067	0.089	0.094	0.044	0.029	0.394	15
14	0.236	0.267	0.265	0.079	0.089	0.088	0.032	0.031	0.499	6
15	0.274	0.272	0.250	0.091	0.091	0.083	0.020	0.041	0.667	3
16	0.300	0.297	0.249	0.100	0.099	0.083	0.016	0.052	0.764	1

To verify the printability with the optimal variables, a cylinder thin-walled component with 20 layers was built (Fig 6). It is found that the cylinder wall also has regular height, width, and good shape. Moreover, no major defects (e.g., cracks and lack of fusions) were found, confirming the efficiency of the optimal process variables.

Fig. 6. The component built with the optimal variables

4. CONCLUSIONS

In this research, the multi-attribute optimization issue in the wire and arc DED process of ER308L stainless steel was resolved to obtained expected attributes of weld tracks for the printing. For that goal, the L16-orthogonal-array Taguchi method were utilized to design the experiment. The impact levels of process variables on the attribute and the accuracy of predictive models were evaluated through the analysis of variance (ANOVA). TOPSIS and DF methods were used to resolve the multi-attribute optimization problem. The findings of this study were drawn as following:

- The predicted models of *WTW*, *WTH*, and α were built with high accuracy (R^2 = 98.92%, 98.77%, and 98.91% for *WTW*, *WTH*, and α, respectively). They can be utilized to predict *WTW*, *WTH*, and α in the whole design area and to predict the optimal set of variables.
- The variable *U* features the most impact on *WTW* and α, meanwhile the variable *I* shows the highest impact on *WTH*.
- Both the TOPSIS and DF methods were utilized to resolve the multi-attribute optimization and given the same optimal solution, {*U* = 23 V, *v* = 300 mm/min, and *I* = 140 A} for the wire-arc DED of ER308L steel.
- The optimal process variables, {*U* = 23 V, *v* = 300 mm/min, and *I* = 140 A}, allows us to build thin-walled components with stable and regular shape, validating their effectiveness for the wire and DED process.

REFERENCES

[1] JAFARI D., VANEKER T.H.J., GIBSON I., 2021, *Wire and Arc Additive Manufacturing: Opportunities and Challenges to Control the Quality and Accuracy of Manufactured Parts*, Materials & Design, 202, 109471, https://doi.org/10.1016/j.matdes.2021.109471.

[2] ZAHIDIN M.R., YUSOF F., ABDUL RASHID SH., MANSOR S., RAJA S., JAMALUDIN M.F., 2023, *Research Challenges, Quality Control and Monitoring Strategy for Wire Arc Additive Manufacturing*, Journal of Materials Research and Technology, 24, 2769–2794, https://doi.org/10.1016/j.jmrt.2023.03.200.

[3] LE V.T., BUI M.C., NGUYEN T.D., NGUYEN V.A., NGUYEN V.C, 2023, *On the Connection of the Heat Input to the Forming Quality in Wire-and-Arc Additive Manufacturing of Stainless Steels*, Vacuum, 209, 111807, https://doi.org/10.1016/j.vacuum.2023.111807.

[4] TOMAR B., SHIVA S., NATH T., 2022, *A Review on Wire Arc Additive Manufacturing: Processing Parameters, Defects, Quality Improvement and Recent Advances*, Materials Today Communications, 31, 103739, https://doi.org/10.1016/j.mtcomm.2022.103739.

[5] SURYAKUMAR S., KARUNAKARAN K.P., BERNARD A., CHANDRASEKHAR U., RAGHAVENDER N., SHARMA D., 2011, *Weld Bead Modeling and Process Optimization in Hybrid Layered Manufacturing*, CAD Computer Aided Design, 43, 331–344, https://doi.org/10.1016/j.cad.2011.01.006.
[6] WANG Z., ZIMMER-CHEVRET S., LÉONARD F., ABBA G., 2021, *Prediction of Bead Geometry with Consideration of Interlayer Temperature Effect for Cmt-Based Wire-Arc Additive Manufacturing*, Welding in the World, 65, 2255–2266, https://doi.org/10.1007/s40194-021-01192-2.
[7] GENG H., XIONG J., HUANG D., LIN X., LI J., 2017, *A Prediction Model of Layer Geometrical Size in Wire and Arc Additive Manufacture Using Response Surface Methodology*, International Journal of Advanced Manufacturing Technology, 93, 175–186, https://doi.org/10.1007/s00170-015-8147-2.
[8] YOUHENG F., GUILAN W., HAIOU Z., LIYE L., 2017, *Optimization of Surface Appearance for Wire and Arc Additive Manufacturing of Bainite Steel*, International Journal of Advanced Manufacturing Technology, 91, 301–313, https://doi.org/10.1007/s00170-016-9621-1.
[9] SARATHCHANDRA D.T., DAVIDSON M.J., VISVANATHAN G., 2020, *Parameters Effect on SS304 Beads Deposited by Wire Arc Additive Manufacturing*, Materials and Manufacturing Processes, 35, 852–858, https://doi.org/10.1080/10426914.2020.1743852.
[10] KUMAR A., MAJI K., 2020, *Selection of Process Parameters for Near-Net Shape Deposition in Wire Arc Additive Manufacturing By Genetic Algorithm*, Journal of Materials Engineering and Performance, 29, 3334–3352, https://doi.org/10.1007/s11665-020-04847-1.
[11] VENKATARAO K., 2021, *The Use of Teaching-Learning Based Optimization Technique for Optimizing Weld Bead Geometry as Well as Power Consumption in Additive Manufacturing*, Journal of Cleaner Production, 279, 123891, https://doi.org/10.1016/j.jclepro.2020.123891.
[12] LE V.T., DOAN Q.T., MAI D.S., BUI M.C., TRAN H.S., VAN TRAN X., 2022, *Prediction and Optimization of Processing Parameters in Wire and Arc-Based Additively Manufacturing of 316L Stainless Steel*, Journal of the Brazilian Society of Mechanical Sciences and Engineering, 44, 394, https://doi.org/10.1007/s40430-022-03698-2.
[13] KANNAN T., YOGANANDH J., 2010, *Effect of Process Parameters on Clad Bead Geometry and its Shape Relationships of Stainless Steel Claddings Deposited by Gmaw*, The International Journal of Advanced Manufacturing Technology, 47, 1083–1095, https://doi.org/10.1007/s00170-009-2226-1.
[14] JINDAL S., CHHIBBER R., MEHTA N.P., 2014, *Effect of Welding Parameters on Bead Profile, Microhardness and H 2 Content in Submerged Arc Welding of High-Strength Low-Alloy Steel*, Proceedings of the Institution of Mechanical Engineers, Part B: Journal of Engineering Manufacture, 228, 82–94, https://doi.org/10.1177-/0954405413495846.
[15] LEE H., KIM J., PYO C., KIM J., 2020, *Evaluation of Bead Geometry for Aluminum Parts Fabricated Using Additive Manufacturing-Based Wire-Arc Welding*, Processes, 8, 1211, https://doi.org/10.3390/pr8101211.